

# Model-based identification of solar coronal mass ejections using deep neural networks

F.A. Iglesias<sup>1,2</sup>, F. Cisterna<sup>1</sup>, M. Sanchez<sup>1</sup>, Y. Machuca<sup>1</sup>, D. Lloveras<sup>1,2</sup>, F. Manini<sup>1,2</sup>, F.M. Lopez<sup>1,2</sup>,  
H. Cremades<sup>1,2</sup> & A. Asensio-Ramos<sup>3</sup>

<sup>1</sup> *Grupo de Estudios en Heliofísica de Mendoza, Universidad de Mendoza, Argentina*

<sup>2</sup> *Consejo Nacional de Investigaciones Científicas y Técnicas, Argentina*

<sup>3</sup> *Instituto de Astrofísica de Canarias, España*

Received: 09 February 2024 / Accepted: 08 May 2024

©The Authors 2024

**Resumen** / Las eyecciones coronales de masa (ECM) son un factor determinante del clima espacial y, por lo tanto, pueden tener impactos tecnológicos y sociales negativos importantes. Para poder predecir su geoeffectividad, es crucial su identificación en imágenes de coronógrafos. En la última década, las redes neuronales profundas (RNP) han experimentado enormes mejoras para resolver diversas tareas relacionadas con la visualización por computadora. Un problema al intentar utilizar RNP para la segmentación de una ECM, es que no existe un conjunto de datos grande y curado en la literatura que pueda utilizarse para el entrenamiento supervisado. Hemos creado un conjunto de datos sintético de imágenes de coronógrafos de ECM que incorpora las características principales de interés, combinando imágenes reales de coronógrafos, con ECM sintéticas obtenidas mediante el modelo geométrico Graduated Cylindrical Shell (GCS). Presentamos el entrenamiento y rendimiento preliminar de una RNP que permite identificar y segmentar la envoltura exterior de una ECM en imágenes de coronógrafos. La RNP se basa en un ajuste fino del modelo MaskR-CNN, y produce una máscara de segmentación similar a la del GCS de la ECM presente en una única imagen diferencial del coronógrafo. Comparamos nuestros resultados con los de otros dos algoritmos clásicos usados para segmentar ECM.

**Abstract** / Coronal mass ejections (CMEs) are a major driver of space weather and thus can have important negative technological and social impacts. To assess their geoeffectiveness once they are ejected, it is crucial their prompt identification in coronagraph images. In the last decade, deep neural networks (DNN) have experienced enormous improvements in solving various machine-vision related tasks. One issue when trying to use DNN for CME segmentation, using coronagraph images, is that no large curated dataset exists in the literature that can be used for supervised training. We have produced a synthetic dataset of CME coronagraph images that incorporates the main features of interest, by combining actual quiet (no CME) coronagraph images with synthetic CMEs simulated using the Graduated Cylindrical Shell (GCS) geometric model. In this work, we present preliminary results of a DNN trained to identify and segment the outer envelope of CMEs. This is done by fine-tuning a pre-trained MaskR-CNN model, to produce a GCS-like mask of the CME, present in a single differential coronagraphic image. We compare our results with two other classic CME segmentation algorithms.

*Keywords* / Sun: coronal mass ejections (CMEs) — techniques: image processing — methods: data analysis

## 1. Introduction

Given the current inability to forecast the occurrence of coronal mass ejections (CMEs), evaluating their geoeffectiveness is crucial. Accurate identification of CMEs in coronagraph images and the characterization of their morphology in three dimensions (3D) is essential for this task. However, up to date, CMEs have been imaged using coronagraphs located at only three different vantage points in the best case, e.g., those of the *Solar and Heliospheric Observatory* (SoHO) and *Solar Terrestrial Relations Observatory* (STEREO) space missions. To overcome this ill-posed problem, the Graduated Cylindrical Shell model (Thernisien et al., 2009) uses a simple croissant-like shell that depends only on six parameters. The GCS model is widely used in the literature to adjust the outer envelope of CMEs observed in differential coronagraph images, acquired simultaneously from two

or three viewpoints. This procedure is almost exclusively done manually, by comparing only morphological aspects. This given that an automatic fit by minimizing the difference between model and measured brightness levels, is difficult because it requires: (a) modeling the rapidly changing CME internal density distribution and its associated brightness, and (b) identifying in the coronagraph images the sections (pixels) belonging to the CME structure and assessing their total brightness. Task (b) is particularly complicated because CMEs can be highly amorphous, and their brightness is noisy and faint compared to an also dynamic background, among other reasons. Moreover, when using differential images to reduce the background influence, different sections of the CME internal structure may appear at various differential brightness levels due to the inhomogeneous 3D velocity field of the CME internal material. This makes

it very difficult or even impossible to identify the true CME outer shell predominant morphology. In this work, we explore deep neural networks to tackle the identification of CMEs using a GCS-based segmentation mask.

Automatic CME identification in coronagraph images and estimation of their basic morphological and kinematic parameters, such as angular width (AW), the central position angle (CPA), the apex distance, and velocity, have been approached using both manual and automated techniques. The manual identification relies on a trained operator, e.g., the Coordinated Data Analysis Workshop (CDAW) Large Angle and *Spectrometric Coronagraph Experiment* (LASCO) CME catalog, and is subjective and unsuitable for real-time applications. The automated approach groups various traditional and machine learning algorithms, which rely on identifying in a single image or a time series, the areas (pixels) belonging to the CME. Some examples of the automated approach are the Solar Eruptive Event Detection System (SEEDS) (Olmedo et al., 2008) and Coronal SEgmentation Technique (CORSET) (Goussies et al., 2010) algorithms, and the CME Automatic detection and tracking with Machine Learning (CAMEL) (Wang et al., 2019) and Alshehhi (Alshehhi & Marpu, 2021) neural network-based methods. The automated methods are based on differential brightness changes and typically do not impose a strong constraint on the identified CME shape. This complicates modeling the identified region using a simply connected shape, like the one derived from parametric models such as the GCS. We propose a DNN-based model to segment individual CME images that produce GCS-like segmentation masks.

## 2. Synthetic CMEs training dataset

It consists of  $1.5 \times 10^5$  synthetic images [515x512] pixels, their associated masks, labels, and bounding boxes for CME and occulter, see Fig. 1. The synthetic images are formed by adding: (1) a background corona randomly selected from a curated database of *STEREO/COR2* differential images with no CME present in the field of view, (2) a synthetic occulter according to the background image, (3) a synthetic CME differential brightness image, and (4) Gaussian noise. The image in (3) is obtained by applying ray tracing to the density distribution derived from the GCS model. Three model evaluations are used, the first (btot) is evaluated with random input parameters from a predefined range, the second (btot\_inner) is evaluated as btot except that the GCS height parameter is multiplied by a random scaling factor in the [0.55–0.85] range, the third (btot\_outer) is evaluated as btot\_inner but using a second scaling of 1.2. The relative intensities of all these components are randomized within a predefined range.

## 3. Deep neural network model for CME segmentation

We use the MASK R-CNN (He et al., 2017) model, designed to perform semantic detection and segmentation of multiple objects in a single image. The architecture of

this model is formed by combining a deep convolutional backbone for feature extraction, a RESNET-50-FPN ([www.pytorch.org/vision/main/models](http://www.pytorch.org/vision/main/models)), followed by a two-channel head. Channel one is a fully connected multilayer perceptron that outputs the object bounding box location and its label. Channel two is a 2-to-4-layer convolutional network that outputs the object mask, i.e., one scalar score value per pixel within the bounding box that quantifies the probability of the pixel to belong to the object. The MASK R-CNN loss is a combination of errors in the inferred boxes, labels and masks. We use fine tuning to train the model. This means that we first load the  $4.6 \times 10^7$  MASK R-CNN parameters pre-trained on the COCO (Common Objects in Context) image dataset ( $8 \times 10^5$  images, 100 classes). After that, we freeze the first two layers, i.e., they are not trained, before doing supervised training in 90% of our synthetic CME dataset. We train for  $1 \times 10^5$  batches of eighth images each, which are randomly rotated and normalized to the [0–1] range before feeding the model. We select the pixel threshold value of 0.5, which minimizes the model test loss (relative difference in the mask areas) on the remaining 10% of the dataset.

## 4. Preliminary Results

For each input image, the trained model produces multiple masks of varied accuracies. This can be due to highly dynamic background structures, slow and/or faint CMEs, or the presence of multiple CMEs simultaneously, see Fig. 2 and 3. To select the appropriate mask for a given image, we do not rely solely on their score (as commonly done in other MASK R-CNN implementations) but use their morphological (AW and CPA) consistency among all the masks found in the images of a time series belonging to the same CME event, see Fig. 2.

CPA and AW for each mask are taken as the median and 95-to-5 percentiles difference of the mask pixel angular distribution around the occulter, respectively. If no consistent mask is found for a given image, then no detection is reported. If there are less than two masks per CME event, the event is left with no detection. As a first validation, we compare the event minimum AW and median CPA computed with our neural segmentation and the values given by the SEEDS and Vourlidis (Vourlidis et al., 2017) catalogs for 35 CMEs taken from the Coronal Mass Ejection Kinematic Database Catalogue (KINCAT) catalog ([www.affects-fp7.eu](http://www.affects-fp7.eu)), see Fig. 4. We expect Vourlidis to be more accurate than SEEDS because events are manually selected, and the CME is masked using the CORSET algorithm. The CPA correlation is high with both catalogs; with the outliers belong to cases where SEEDS (see an example in Fig. 5) or Vourlidis (see an example in Fig. 6) detections failed. The AW correlation is much lower, with our estimations being typically larger than Vourlidis and lower than SEEDS (which is generally unreliable because it is pixel-based). An extra comparison with AW in the KINCAT catalog using GCS estimations will quantify AW estimation errors.

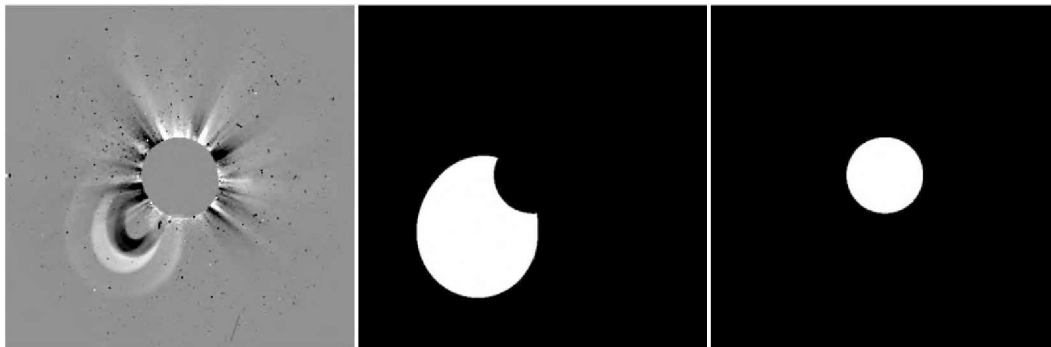


**Fig. 1.** Synthetic GCS-based differential brightness coronagraph image (*left*) and its associated binary masks for labels CME (*center*) and occulter (*right*).

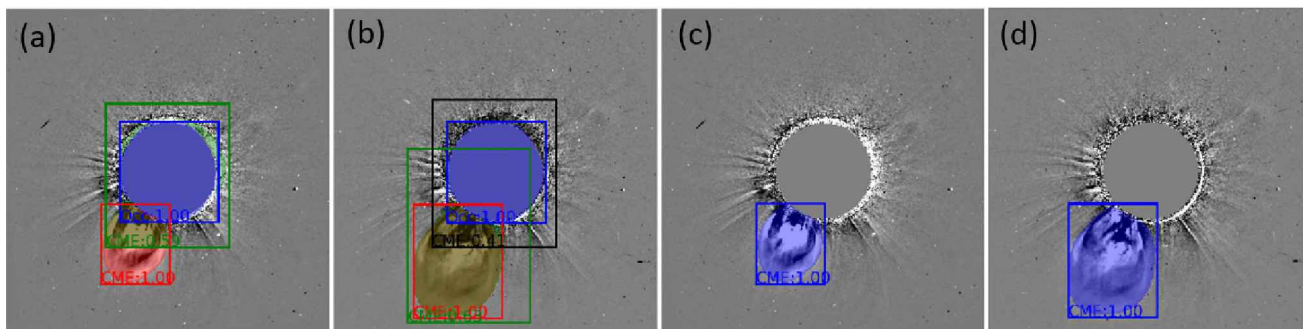


**Fig. 2.** Masks found in real *LASCO C2* differential images acquired on 24 April 2013 at 06:59 UT (a) and 07:23 UT (b). We show only masks with score  $> 0.25$ . The final selected masks are presented in panels (c) and (d). The corresponding rectangular bounding boxes are computed from the masks using the Python function `cv2.BOUNDINGRECT()`.

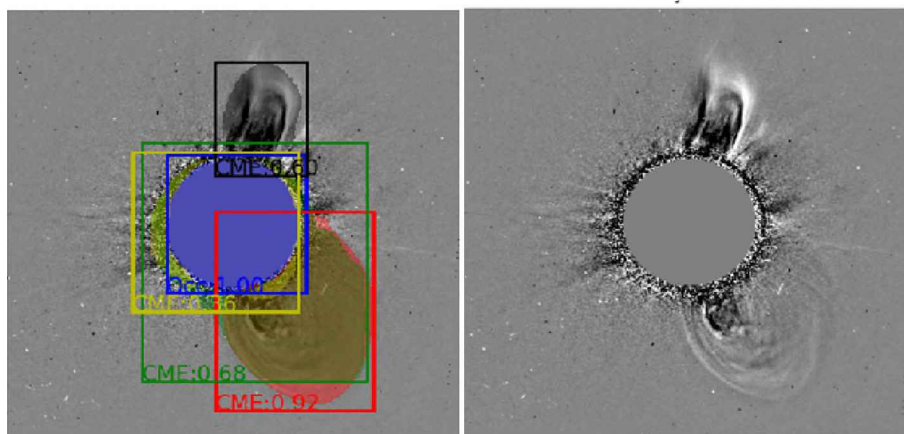


**Fig. 3.** *SOHO/LASCO C2* 24 April 2013 at 04:23 UT showing the masks found for two CMEs

## 5. Conclusions and future work

Based on these preliminary results, we conclude:

- Our synthetic CME images do contain the main features that allow the neural network to segment the CME outer envelope using a simple, fully connected geometric mask in most of the cases.
- The MaskR-CNN model architecture, particularly the depth of the convolutional backbone, seems enough to capture the relevant image features to segment CMEs.
- Basic morphological parameters such as CPA and

AW derived from our GCS-based mask are in agreement with those derived from other methods. However, while the CPA correlation is high ( $> 85\%$ ), the dispersion of the derived AWs is more sensitive to the correct shape.

- Cases of wrong detections with our NN seem to be related to CMEs that present strong elements not included in the synthetic dataset, such as leading shock or deflected streamers.

To further improve the segmentation quality we plan to:

- Increase dataset size and include in the synthetic images other important elements, such as the leading

## Model-based identification of CMEs using DNN

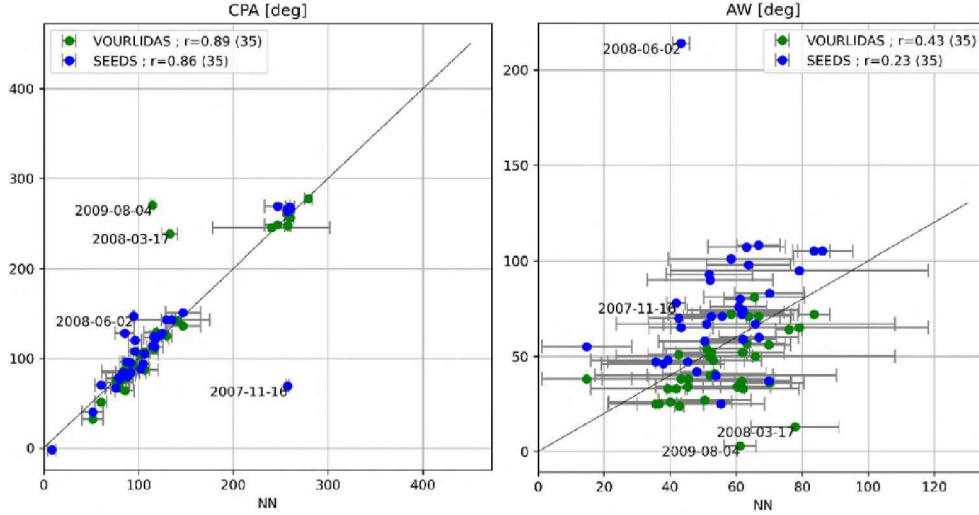


**Fig. 4.** CPA (left) and AW (right) estimated with SEEDS and Vourlidas (see the legend) vs. our estimation (horizontal axis). The outliers in CPA are shown in Figs. 5 to 8.

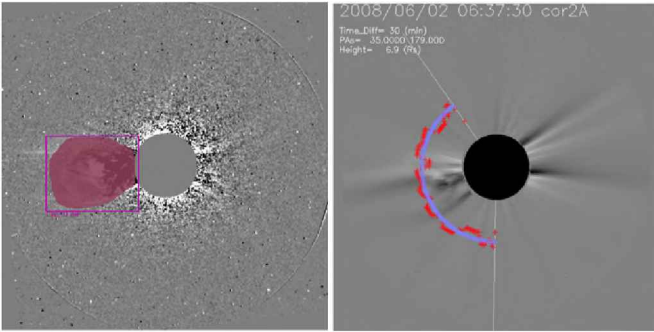


**Fig. 5.** SECCHI/COR2-A 02 June 2008 at 06:37 UT. Our (left) and SEEDS (right) wrong detection (AW too large).

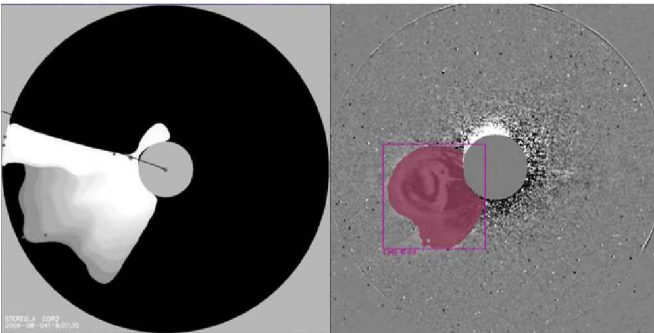


**Fig. 6.** SECCHI/COR2-A 04 August 2009 at 22:07 UT. Vourlidas (left) failed detection vs. ours (right). Vourlidas reports outflowing background material, which is likely the cause of the false detection.

shock and deflected lateral streamers.

- Use a neural model that can ingest many time-instants simultaneously.
- Compare the mask derived with our NN and the other algorithms with the masks derived by manual GCS fitting, considering the latter as a ground truth. This can help to devise which method derives better CME properties such as the AW.

*Acknowledgements:* FAI, MS, and FC are supported by The Max Planck Partner Group between the University of Mendoza and the Max Planck Institute for Solar System Research (MPS).

## References

Alshehhi R., Marpu P.R., 2021, *Solar Phys.*, 296, 104  
 Goussies N., et al., 2010, *Solar Phys.*, 262, 481  
 He K., et al., 2017, arXiv e-prints, arXiv:1703.06870  
 Olmedo O., et al., 2008, *Solar Phys.*, 248, 485  
 Thernisien A., Vourlidas A., Howard R.A., 2009, *Solar Phys.*, 256, 111  
 Vourlidas A., et al., 2017, *ApJ*, 838, 141  
 Wang Y., et al., 2019, *ApJ*, 881, 15